GEOPHYSICAL RESEARCH LETTERS, VOL. 40, 5698–5703, doi:10.1002/2013GL057652, 2013

Estimation of ICESat intercampaign elevation biases from comparison of lidar data in East Antarctica

M. A. Hofton,[1] S. B. Luthcke,[2] and J. B. Blair[3]

Received 13 August 2013; revised 22 October 2013; accepted 24 October 2013; published 11 November 2013.

[1] The Ice, Cloud, and land Elevation Satellite (ICESat) laser campaign elevation biases are estimated from an analysis of ICESat and airborne Land, Vegetation, and Ice Sensor lidar intrasensor and intersensor elevation differences from two regions of the Antarctic ice sheet that experienced minimal surface elevation change. Elevation observations are corrected for a combination of accumulation, melting, and firn densification processes and glacial isostatic adjustment. ICESat elevations are adjusted for the saturation and Gaussian-Centroid corrections. Relative to laser campaign L3I, biases are found to be less than ∼8 cm, except for campaign L2E at 14.72 cm corresponding to the time of a significant accumulation anomaly in East Antarctica. The intercampaign bias trend estimated from intersensor elevation differences computed over campaigns L2A to L2F (September 2003 to October 2009) excluding L2E is 1.04 ± 0.48 cm/yr. The intercampaign bias trend represents a correction to ICESat derived Antarctica mass balance of 117 ± 53 Gt/yr. **Citation:** Hofton, M. A., S. B. Luthcke, and J. B. Blair (2013), Estimation of ICESat intercampaign elevation biases from comparison of lidar data in East Antarctica, *Geophys. Res. Lett.*, *40*, 5698–5703, doi:10.1002/2013GL057652.

1. Introduction

[2] The presence of time-variable biases in lidar surface elevation observations are a potential source of error in the determination of surface elevation change. Data from NASA's Ice, Cloud, and land Elevation Satellite (ICESat) must be corrected for intercampaign (time-variable) elevation biases in order to accurately determine interannual ice sheet surface elevation change [e.g., *Shepherd et al.*, 2012; *Siegfried et al.*, 2011; *Gunter et al.*, 2009]. ICESat was a spaceborne lidar that operated from 2003 to 2009 collecting elevation profiles in 18 ∼monthlong periods 2 to 3 times per year. The ICESat intercampaign biases (ICBs) have been estimated using several approaches. The most recent study by *Shepherd et al.* [2012] uses ICBs derived from the most current ICESat data over midlatitude oceans and estimated an apparent ICB trend of 0.65 cm/yr when corrected for sea level rise of 0.3 cm/yr (2003–2008). However, it is unclear if the ICBs determined from low-albedo ocean lidar observations are applicable to higher-albedo land ice data. Here we compute ICESat ICBs using intra- (ICESat to ICESat) and inter- (ICESat to airborne) lidar sensor elevation difference observations from the Antarctic ice sheet. To minimize corruption of the ICBs by real surface elevation change, we identify two areas of the ice sheet where modeled elevation changes due to climate-related surface processes are small. The ICBs are corrected for the effects of these climate-related processes, as well as global isostatic adjustment (GIA) and the ICESat saturation and Gaussian-Centroid (G–C) corrections [*National Snow and Ice Data Center*, 2013]. Differences between ICB solutions are assessed and their impacts on existing ice mass balance investigated. Intersensor comparisons use data from NASA's Land, Vegetation, and Ice Sensor (LVIS) [*Blair et al.*, 1999].

2. Methods

2.1. ICESat Intrasensor Comparisons

[3] We estimate ICBs from a comparison of near-coincident ICESat elevation measurements in Antarctica. The ICESat single beam lidar operated at 1064 nm and utilized elliptical footprints with a major axis of 51–149 m and an eccentricity of 0.48–0.92 m. Footprints are separated by ∼170 m along track. Elevation data products from the ICESat GLA06 release 633 files are used, and to which we apply the saturation and G–C corrections. Data from all 18 ICESat campaigns are included in the analysis (Table 1), none are excluded on the basis of the orbit pattern during a campaign. ICESat elevation and elevation change accuracy goals were 15 cm (single shot) and 2 cm/yr averaged over 100 × 100 km regions [*Zwally et al.*, 2002].

[4] In order to minimize the influence of surface elevation fluctuations due to climate-related surface processes on our ICB estimates, we have used the model results of *Ligtenberg et al.* [2011] to identify an area on the Antarctic Ice Sheet where spatial and temporal variations due to these processes are smallest. The surface elevation fluctuations were derived from a firn densification model driven by estimates of surface mass balance, temperature, wind speed, and processes associated with liquid water output by the regional atmospheric climate model RACMO2/ANT, at ∼27 km resolution and 48 h intervals for 1979–2010 [*Ligtenberg et al.*, 2011]. Using the least squares regression per model output grid cell, we calculated the linear elevation change for the duration of the ICESat mission and identified cells where the trend and root-mean-square (RMS) of the residuals are smallest. Figure 1 shows the location of an area of 393,765 km^2 on the East Antarctic ice sheet (EAIS) where the estimated annual trends are less than ±2.25 cm/yr and the residual RMS between the model predictions and

[1]Department of Geographical Sciences, University of Maryland, College Park, Maryland, USA.
[2]Code 698, NASA Goddard Space Flight Center, Greenbelt, Maryland, USA.
[3]Code 694, NASA Goddard Space Flight Center, Greenbelt, Maryland, USA.

Corresponding author: M. A. Hofton, Department of Geographical Sciences, University of Maryland, Lefrak Hall, College Park, MD 20741, USA. (mhofton@umd.edu)

0094-8276/13/10.1002/2013GL057652

Table 1. Number of Lidar Footprints and Intrasensor or Intersensor Near-Coincident Footprints[a]

ICESat Campaign	Dates[b]	Days	Lidar Footprints, EAIS			Lidar Footprints, 86S		
			Total	Versus L3I	Avg/Cell	Total	Versus LVIS	Avg/Cell
L1A	2/20/03 to 3/20/03	38	394,144	1,734	34	13,480	12,329	1482
L2A	9/25/03 to 11/18/03	55	591,574	40,555	652	24,042	22,087	2613
L2B	2/17/04 to 3/21/04	33	353,222	39,923	617	14,494	13,247	1592
L2C	5/18/04 to 6/21/04	35	358,981	45,412	695	14,623	13,420	1639
L3A	10/3/04 to 11/8/04	37	392,429	47,609	776	16,446	15,112	1835
L3B	2/18/05 to 3/24/05	36	379,618	48,313	734	15,908	14,551	1763
L3C	5/20/05 to 6/23/05	35	368,817	18,821	334	15,565	14,184	1725
L3D	10/21/05 to 11/24/05	34	361,945	56,484	892	14,585	13,286	1611
L3E	2/22/06 to 3/28/06	34	365,426	58,986	914	14,575	13,361	1629
L3F	5/24/06 to 6/26/06	34	360,041	30,618	524	13,525	12,412	1506
L3G	10/25/06 to 11/27/06	34	363,773	34,006	518	15,387	14,042	1713
L3H	3/12/07 to 4/14/07	34	368,828	49,969	814	15,101	13,789	1678
L3I	10/02/07 to 11/05/07	34	360,333	768	15	14,649	13,358	1630
L3J	2/17/08 to 3/21/08	34	363,662	45,447	695	14,534	13,317	1619
L3K	10/04/08 to 10/19/08	15	157,053	5,052	134	6,705	6,133	749
L2D	11/25/08 to 12/17/08	23	240,433	28,609	482	10,211	9,352	1140
L2E	3/9/09 to 4/11/09	34	356,773	45,042	699	13,970	12,762	1560
L2F	9/30/09 to 10/11/09	12	114,517	6,628	176	4,606	4,183	510

[a]In the East Antarctic ice sheet (EAIS) and 86S (110°E to 155°E) study regions for each ICESat campaign, including the average number of observations per 100 × 100 km (EAIS) or 2 × 50 km (86S) grid cell.
[b]Dates are formatted as month/day/year.

linear fit are <1.00 cm. The modeled mean surface elevation change during the ICESat mission in this region is –0.03 ± 0.14 cm/yr. Over 6 million elevations from the 18 campaigns are presented in this area (Table 1).

[5] Within the EAIS study region, we compute ICESat to ICESat elevation differences between near-coincident footprints binned by ICESat campaign and 100 × 100 km cells, the smallest size with a minimum of a few hundred near-coincident measurements per campaign (Table 1). The elevation differences of each campaign relative to L3I are estimated for each grid cell. The overall EAIS study region ICBs are then calculated from the arithmetic average of the 100 km cell results with an error estimate derived from the standard deviation. Only footprints within 40 m of each other are compared in order to limit the effects of slope on the elevation differences. This yields an average of 33,554 near-coincident footprints per campaign (Table 1) after filtering using a 5σ edit (~1 m) on the elevation differences. This filtering is adequate to remove elevations that could be affected by, for example, atmospheric forward scattering [e.g., *Fricker et al.*, 2005] and minor issues such as errors in the pulse fitting routines or postprocessing elevation corrections. The mean distance between footprint pairs is ~25 ± 10 m.

[6] Although we minimize the influence of climate-related surface processes on our ICBs by selecting a "quiet zone" in which to perform our comparisons, we also subtract the *Ligtenberg et al.* [2011] model surface elevation changes at the times and location of each footprint from the ICESat elevations prior to calculating ICBs. We apply a GIA correction to trends estimated from the ICBs using the results of the IJ05_R2 model [*Ivins and James*, 2005] and corresponding to a 65 km thick lithosphere and upper and lower mantle viscosities of 0.2×10^{21} Pa s and 1.5×10^{21} Pa s. The average surface elevation trend due to GIA in the study region is –0.04 ± 0.01 cm/yr.

2.2. LVIS/ICESat Intersensor Comparisons

[7] As part of NASA's Operation IceBridge, high-altitude flights of NASA's LVIS swath-mapping lidar circumnavigated the South Pole collecting a ~2 km wide swath of surface elevation data close to latitude 86S using ~20 m wide footprints that are contiguous along and across track. Similar to ICESat, the LVIS operates at a wavelength of 1064 nm and digitizes both the outgoing and returning laser waveforms to facilitate the derivation of precise elevations for every footprint. Typical LVIS ice sheet elevation precision and accuracy are at the decimeter level [*Hofton et al.*, 2008].

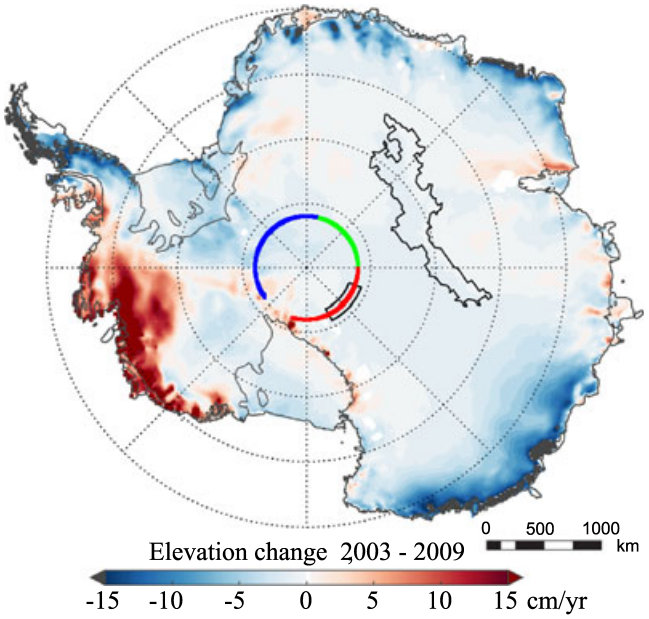

Figure 1. Linear elevation change, February 2003 to October 2009, estimated using the least squares regression per model output grid cell from the results of *Ligtenberg et al.* [2011] due to climate-related surface processes. Locations of EAIS and 86S study regions are outlined in gray. The LVIS 86S flights are shown in blue (2009), red (flight 1, 2010), and green (flight 2, 2010).

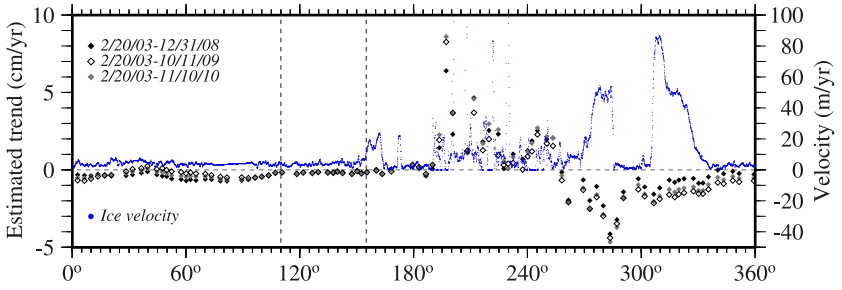

Figure 2. Linear elevation change at 86S estimated using the least squares regression per model output grid cell for three time periods relative to the beginning of the ICESat altimetry (diamonds) from the results of *Ligtenberg et al.* [2011]. Static ice velocity (blue) is also shown. The area of 86S where surface elevation changes are consistent over the three time periods and ice velocity is low lies between the dashed lines at 110°E and 155°E.

[8] The 86S LVIS data collections were flown on 30 October 2009, 4 November 2010, and 10 November 2010 (Figure 1). The 86S flight line offers a unique crossover observation opportunity with ICESat as it is the maximum latitudinal extent of the near-polar inclination satellite orbit. The convergence of ICESat altimeter ground tracks along this 86S comparison zone produces the maximum number of crossover observations with the ~2 km wide LVIS swath.

[9] To identify the segment of the LVIS flight zone likely to be the least influenced by surface elevation changes due to climate-related surface processes, we again use the model results of *Ligtenberg et al.* [2011] as discussed previously in identifying the ICESat intrasensor study region. In addition, we use ice velocity data derived from satellite radar interferometry [*Rignot et al.*, 2011] to apply an additional constraint to minimize the potential influence of velocity variations on surface elevation change. Figure 2 shows the surface elevation change trends estimated from the model results of *Ligtenberg et al.* [2011] between 85.9°S and 86.1°S and static ice velocity for the area within the LVIS swath. Surface elevation trends are estimated for three time periods relative to the beginning of the ICESat altimetry data and ending: (1) 31 December 2008, prior to an exceptional snowfall event in East Antarctica in early 2009 [*Shepherd et al.*, 2012; *Luthcke et al.*, 2013], (2) 11 October 2009, the last day of ICESat altimetry observations, and (3) 10 November 2010, the last day of the LVIS 86S observations.The area of the LVIS swath where model surface elevation changes is both low magnitude and consistent for the three considered time periods and where ice velocity is also low in magnitude lies between 110°E and 155°E longitude (Figure 2).

[10] To estimate ICBs, we compare near-coincident LVIS and ICESat footprints between 110°E and 155°E. We utilize ICESat GLA06 release 633 data product files from all 18 campaigns to which the ICESat saturation and G–C corrections are applied. ICESat elevations are compared to the LVIS Level 2 "low" elevations which represent the mean elevation of the lowest reflecting surface in the footprint. LVIS footprints where multiple reflecting surfaces are likely present are not included. Within the ~2 km by 350 km area between 110°E and 155°E at 86S, there are over 252,406 ICESat and 1,551,752 LVIS footprints (Table 1). We compute ICESat to LVIS elevation differences between near-coincident footprints binned by ICESat campaign and 2 × 50 km long cells along the length of the LVIS swath. To emulate the analysis performed in the EAIS study region, near-coincident ICESat and LVIS footprints whose centers lie within 40 m of each other are compared resulting in at least 4183 (L2F/LVIS) and as many as 22,087 (L2A/LVIS) differences (Table 1). The mean distance between footprint pairs is 7±3 m. As discussed previously, filtering to remove elevations affected by forward scattering or other issues are performed on the differences using a 5σ edit.

[11] To minimize the impact on elevation differences associated with footprint separation and surface slope, we use the LVIS swath surface elevations to correct for long-wavelength topography prior to extracting the elevation differences between overlapping footprints. The long-wavelength topography, S, is given by the following, where x and y are the positions of the LVIS surface elevation observations in a local reference frame:

$$S = A + Bx + Cy + Dxy + Ex^2 + Fy^2. \quad (1)$$

The coefficients A through F are estimated using the LVIS data in 1 km long cells. S is removed from both the LVIS and ICESat elevations prior to calculating the elevation differences at footprint locations. We also subtract the

Table 2. ICESat ICBs From Intersensor and Intrasensor Comparisons in the EAIS and 86S Study Regions Including Corrections for Climate-Related Surface Processes and ICESat Saturation and G–C Errors[a]

ICESat Campaign	Intercampaign Bias, Relative to L3I (cm)		
	86S	EAIS	*Shepherd et al.* [2012]
L1A	–1.14 ± 1.63	–5.08 ± 5.52	–
L2A	3.22 ± 1.84	0.41 ± 5.46	–5.1 ± 1.4
L2B	–1.03 ± 4.27	–1.56 ± 4.28	–3.6 ± 1.4
L2C	7.09 ± 5.48	2.39 ± 5.65	2.1 ± 5.3
L3A	–2.66 ± 4.00	–6.73 ± 3.88	–2.4 ± 0.9
L3B	–2.46 ± 3.08	–5.10 ± 4.59	–2.1 ± 1.1
L3C	–3.55 ± 3.85	–6.20 ± 4.69	1.1 ± 1.5
L3D	1.60 ± 2.53	–3.22 ± 4.22	0.8 ± 0.9
L3E	1.75 ± 1.64	–1.12 ± 4.45	0.8 ± 0.7
L3F	–2.18 ± 2.26	–4.85 ± 4.91	0.0 ± 1.1
L3G	3.21 ± 0.82	–1.12 ± 4.91	2.1 ± 0.7
L3H	1.16 ± 1.81	0.07 ± 3.03	1.5 ± 0.9
L3I	0.00 ± 3.20	0.00 ± 3.30	0.0 ± 0.9
L3J	3.45 ± 2.31	1.33 ± 5.24	–1.0 ± 1.3
L3K	6.23 ± 2.59	3.14 ± 3.40	–0.2 ± 1.4
L2D	7.71 ± 1.51	7.29 ± 4.46	1.8 ± 1.8
L2E	14.72 ± 3.03	13.93 ± 4.89	5.3 ± 4.4
L2F	7.43 ± 2.84	4.21 ± 4.35	–1.2 ± 1.3

[a]Results of *Shepherd et al.* [2012] are corrected for sea level rise of 0.3 cm/yr. ICBs are relative to L3I.

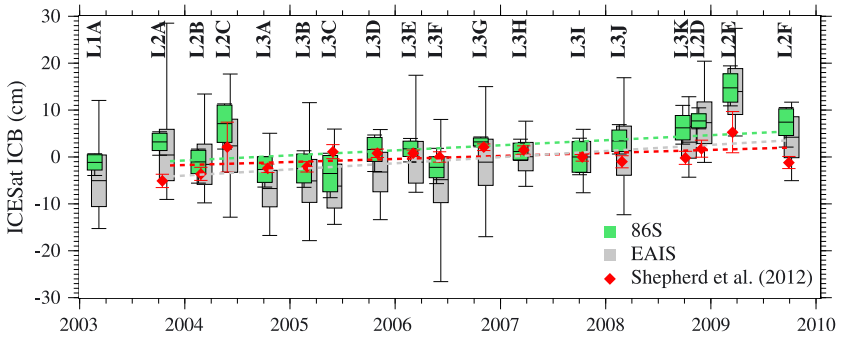

Figure 3. ICESat ICBs relative to L3I in the 86S (green) and EAIS (gray) study regions. Elevations are corrected using the model results of *Ligtenberg et al.* [2011] and the saturation and G–C corrections. Colored boxes represent 1σ variation about the mean. Whiskers indicate the data extremes of each comparison. Results used in *Shepherd et al.* [2012] (red) are corrected for sea level rise of 0.3 cm/yr and are relative to L3I but do not have the G–C correction applied. The error bars represent the RMS of each estimate. Trends fit to the L2A to L2F ICBs (excluding L2E) are shown as dashed lines.

Ligtenberg et al. [2011] model surface elevation changes at the times and location of each footprint from the lidar elevations before calculating ICESat ICBs. The elevation biases between each ICESat campaign and the LVIS campaign are estimated for each of the seven ~2 × 50 km cells between 110°E and 155°E. In order to compute ICESat ICBs relative to L3I, the ICESat to LVIS estimated biases for the L3I campaign are removed from the biases estimated for each of the other ICESat campaigns. ICESat ICBs are computed for each campaign as the arithmetic average of all the biases estimated for each of the 2 × 50 km cell relative to L3I. The error estimate for each ICB is computed as the standard deviation of the 2 × 50 km cell biases. We apply a GIA correction to trends estimated from the ICBs using the results of the IJ05_R2 model. The average surface elevation trend due to GIA in the study region is –0.02 ± 0.01 cm/yr.

2.3. Error Analysis

[12] The estimates for the ICESat ICBs and trends estimated from these biases contain both noise-only and systematic errors. The noise-only error estimates are provided as error bars in the tables and figures. The noise-only error estimate for each ICB is calculated from the standard deviation of the ICBs computed for each of the study region cells. For the EAIS area, there are an average of fifty-six 100 × 100 km cells with enough near-coincident footprints to calculate a valid ICB for each campaign, while for the 86S area, there are seven 2 × 50 km cell ICBs used in the calculation. For trends fit to the ICBs, the formal error from the least squares estimation is used as the noise-only error estimate.

[13] Systematic errors are considerably more difficult to estimate. The ICESat ICB estimates may be contaminated by errors in the ICESat data including corrections (e.g., saturation and G–C corrections), and signals associated with surface elevation changes due to climate-related surface processes or GIA. Differencing ICB and ICB trend estimates from the two study regions provides a means to gauge systematic errors. The difference removes common errors, which we assume are dominated by the ICESat ICBs, but also removes any remaining common surface elevation change errors. Still, the difference provides an important estimate of noncommon systematic errors arising from the remaining uncorrected and unmodeled ICESat data errors (including those that could be caused by the spatial variation of the ICBs themselves given the two study regions are more than 1000 km apart), and surface elevation changes after our attempt to minimize the impact through the selection of quiet zones and the application of the model for climate-related surface processes.

3. Results

[14] The ICESat ICB estimates from the EAIS and 86S study regions are shown in Table 2 and Figure 3 along with the ICBs from *Shepherd et al.* [2012] determined from the release 633 ICESat elevations between ±66° latitude. The *Shepherd et al.* [2012] ICBs are corrected for sea level rise of 0.3 cm/yr (2003–2008) and normalized to L3I but do not include the ICESat G–C correction. The ICBs determined from the EAIS and 86S study regions agree to within the

Table 3. ICB Trends for Time Periods L2A to L2F (Excluding L2E) and L2A to L2D (the Time Period Used in *Shepherd et al.* [2012]), Applying Various Elevation Corrections[a]

	L2A to L2F, Excluding L2E (cm/yr)			L2A to L2D (cm/yr)	
Data Set	86S	EAIS	86S–EAIS	86S	EAIS
No FDM, no G–C	1.57 ± 0.47	1.81 ± 0.38	–0.25 ± 0.25	1.91 ± 0.52	2.17 ± 0.40
No FDM, G–C	1.06 ± 0.53	1.32 ± 0.48	–0.26 ± 0.25	0.94 ± 0.61	1.18 ± 0.56
FDM, no G–C	1.59 ± 0.43	1.80 ± 0.39	–0.21 ± 0.21	1.88 ± 0.48	2.23 ± 0.39
FDM, G–C	1.08 ± 0.47	1.30 ± 0.45	–0.22 ± 0.21	0.91 ± 0.55	1.25 ± 0.53
FDM, G–C, GIA	**1.04 ± 0.48**	1.28 ± 0.46	–0.24 ± 0.21	**0.87 ± 0.56**	1.23 ± 0.54

[a]Trends fit to the differences between the 86S and EAIS ICB solutions for L2A–L2F (excluding L2E) are also shown. Preferred solutions are in bold. Firn densification modeling (FDM) refers to the model results of *Ligtenberg et al.* [2011].

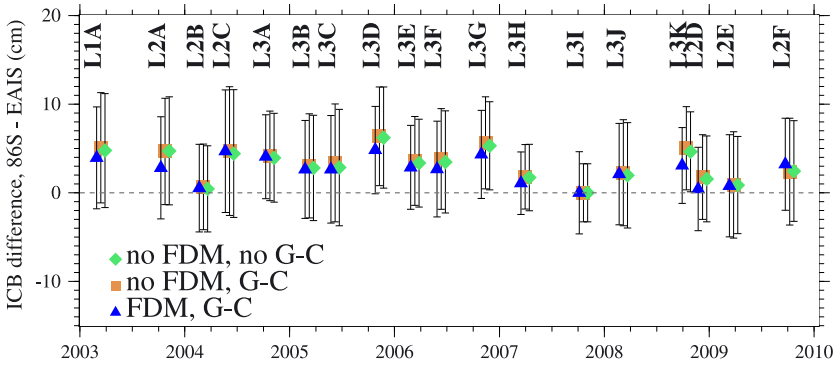

Figure 4. Differences between ICB estimates from the EAIS and 86S study regions with corrections applied. Error bars represent the root-sum-square of the solutions. FDM refers to the model results of *Ligtenberg et al.* [2011] for climate-related surface processes.

noise-only error estimates in all cases (Figure 3). Results from 86S where a larger number of near-coincident footprints are available have smaller noise-only estimated errors for all campaigns (Figure 3). The *Shepherd et al.* [2012] ICBs show similar patterns to the biases determined from our two study regions and in general are nearly within the error estimates, except most notably L2E (Figure 3).

[15] The trends estimated from the suite of ICB solutions studied are presented in Table 3. We exclude the ICB for the L2E campaign from the trend estimate because it corresponds to the time of an accumulation anomaly in East Antarctica [*Shepherd et al.*, 2012; *Luthcke et al.*, 2013]. We also exclude the ICB for the L1A campaign from the trend estimate because of poor calibration for this first ICESat campaign that was prior to the refinement of on-orbit techniques to optimize mission performance. In addition, we include a trend estimate for the period L2A to L2D to provide a direct comparison to the results of *Shepherd et al.* [2012]. All ICBs are weighted equally in the trend estimate. All data from L2A are included, containing the nonrepeat period data. The ICB differences between the EAIS and 86S solutions are shown in Figure 4 in order to compare the impact of the application of the G–C correction and model elevation changes of *Ligtenberg et al.* [2011]. The trends estimated from the L2A to L2F ICB solution differences are also shown in Table 3. The G–C correction decreases the ICB trends from both regions (∼ –0.50 cm/yr for L2A–L2F and –0.99 cm/yr for L2A–L2D) (Table 3). Application of the model results of *Ligtenberg et al.* [2011] for the effects of climate-related surface processes has a small impact on the trends (<0.07 cm/yr) but does reduce the discrepancy between the two solutions indicating that it reduces the remaining systematic surface elevation change error. The impact of GIA is less than 0.04 cm/yr.

4. Discussion

[16] The trend associated with the ICESat ICBs is an important quantity that has been used to correct ice mass balance solutions estimated from ICESat surface elevation observations, for example, as part of the Ice sheet Mass Balance Intercomparison Experiment as summarized by *Shepherd et al.* [2012]. Our preferred solution for the ICESat ICB trend for L2A to L2F (September 2003 to October 2009), excluding L2E, is 1.04 ± 0.48 cm/yr (Table 3). This is computed from the 86S study region using intersensor differences from which long-wavelength topography is removed and to which corrections for ICESat elevation errors and elevation changes due to climate-related surface processes and GIA are applied. A comparison of our preferred solution with that obtained from the EAIS analysis shows 0.24 cm/yr agreement (Table 3). The agreement is well within the error estimate and indicates noncommon systematic errors are not a significant error source. However, while we have attempted to reduce systematic surface elevation change error by comparing data in areas where elevation fluctuations due to climate-related surface processes are minimized, as well as applying model predictions for these changes and GIA, common systematic surface elevation change errors could still exist that are not accounted for in our error estimate and not observable in our solution difference.

[17] The time period of the ice mass balance study of *Shepherd et al.* [2012] is L2A to L2D (October 2003 to December 2008). Our preferred ICB trend for this time period is 0.87 ± 0.55 cm/yr (Table 3). The trend used by *Shepherd et al.* [2012] in the computation of ice mass balance results is 0.65 cm/yr, approximately equivalent to 73 Gt/yr for Antarctica [*Shepherd et al.*, 2012]. Using this relationship, our trend of 0.87 ± 0.55 cm/yr is equivalent to ∼98±62 Gt/yr for Antarctica. For L2A to L2F (excluding L2E), our trend is equivalent to ∼117±53 Gt/yr.

[18] To understand whether or not our ICB trend solution is congruent with Antarctica ice mass balance estimates, we simply apply the additional mass correction to the *Shepherd et al.* [2012] Antarctic ice sheet estimates for the time period October 2003 to December 2008. The *Shepherd et al.* [2012] ICESat mass balance estimates for Antarctica are 49 ± 69 Gt/yr and 6 ± 72 Gt/yr assuming ICB trends of 0.0 cm/yr and 0.65 cm/yr. *Shepherd et al.* [2012] use these two estimates to calculate the mean Antarctic ice sheet estimate of 21 ± 71 Gt/yr. The additional mass corrections to the *Shepherd et al.* [2012] estimates suggested by our ICB trend are –98 Gt/yr and –25 Gt/yr. Applying these to the individual estimates, we obtain –49 ± 69 Gt/yr and –19 ± 72 Gt/yr. The updated mean Antarctic ICESat estimate is –34 ± 71 Gt/yr, improving the agreement between the ICESat estimate and the mean GRACE estimate of –57 ± 50 Gt/yr [*Shepherd et al.*, 2012]. However, only the first of the two *Shepherd et al.* [2012] estimates uses ICESat release 633 data, and further investigation of the differences between ICESat data releases is required in order

to fully assess the applicability of our ICBs to older ICESat data and the overall *Shepherd et al.* [2012] Antarctic ICESat mass balance estimate.

[19] The *Shepherd et al.* [2012] mass balance solution for Greenland also utilizes ICESat release 431, thus making an assessment of the impact of our new ICB solution in Greenland difficult to determine. In Greenland, an ICB trend of 0.6 cm/yr is equivalent to ∼9 Gt/yr [*Zwally et al.*, 2011]. Using this relationship, our ICB trend of 0.87±0.55 cm/yr is equivalent to ∼13±8 Gt/yr. Applying the additional mass correction of our preferred ICB trend to the *Shepherd et al.* [2012] Greenland mass balance estimates of –185 ± 8 Gt/yr and –197 ± 23 Gt/yr (that assumed ICB trends of 0.6 cm/yr [*Zwally et al.*, 2011] and 0.65 cm/yr [*Shepherd et al.*, 2012]), these become –189 ± 8 Gt/yr and –200 ± 23 Gt/yr. The mean of –195 ± 24 Gt/yr is slightly closer to the mean GRACE estimate of –228 ± 30 Gt/yr [*Shepherd et al.*, 2012].

[20] It should be noted that the simple application of a linear ICB trend to postsolution correct the ICESat ice mass balance estimate does not take into account the spatial and temporal density of the ICESat data in the computation of surface elevation change. It also does not take into account that the generation of time-varying ICB trends are more appropriate to correct elevation change rates over shorter time periods. It is likely that our new time-varying ICB estimate could be used to correct ICESat data globally and that the differences between various ICB solutions could be used as a guide to estimate the magnitude of any systematic errors. However, the proper way to account for ICESat ICBs is to apply them to the ICESat elevation data prior to any procedure to estimate elevation change for mass balance calculations. Still, given the difference between our new estimate of the ICB trend and that used in *Shepherd et al.* [2012], our simple postsolution corrections calculated here indicate improved agreement between ICESat and Gravity Recovery and Climate Experiment (GRACE) mass balance estimates are achievable when our new ICB solutions are applied.

5. Conclusions

[21] We estimate ICESat ICBs utilizing lidar data collected in Antarctica from two areas with minimal surface elevation change. Our ICBs are similar in pattern and, in general, within the error estimates of ICBs presented by *Shepherd et al.* [2012] obtained from an analysis of ICESat data over midlatitude oceans. Our preferred solution for the ICB trend from the 86S region agrees with that obtained from the EAIS region within the error estimate. The ICBs should be applied to the ICESat elevation data prior to any procedure to estimate elevation change for ice mass balance calculations; however, the simple application of a linear trend fit to our ICB solutions reduces the Antarctica and Greenland ICESat and GRACE ice mass balance differences of *Shepherd et al.* [2012].

[22] **Acknowledgments.** The authors would like to thank S. Ligtenberg, E. Ivins, M. Beckley, C. Shuman, an anonymous reviewer, and J. Stroeve for their input and reviews. M.H. was supported by grant NNX11AH69G.

[23] The Editor thanks Christopher Shuman and Beata Csatho for their assistance in evaluating this paper.

References

Blair, J. B., D. Rabine, and M. Hofton (1999), The laser vegetation imaging sensor: A medium-altitude, digitisation-only, airborne laser altimeter for mapping vegetation and topography, *ISPRS J. Photogramm. and Rem. Sens.*, *54*, 115–122.

Fricker, H., et al. (2005), Assessment of ICESat performance at the salar de Uyuni, Bolivia, *Geophys. Res. Lett.*, *32*, L21S06, doi:10.1029/2005GL023423.

Gunter, B., et al. (2009), A comparison of coincident GRACE and ICESat data over Antarctica, *J. Geod.*, *83*, 1051–1060, doi:10.1007/s00190-009-0323-4.

Hofton, M. A., et al. (2008), Assessing the performance of 20–25 m footprint waveform lidar data collected in ICESat data corridors in Greenland, *Geophys. Res. Lett.*, *35*, L24501, doi:10.1029/2008GL035774.

Ivins, E. R., and T. S. James (2005), Antarctic glacial isostatic adjustment: A new assessment, *Antarct. Sci.*, *17*, 541–553, doi:10.1017/S0954102005002968.

Ligtenberg, S. R. M., et al. (2011), An improved semi-empirical model for the densification of Antarctic firn, *The Cryosphere*, *5*, 809–819, doi:10.5194/tc-5-809-2011.

Luthcke, S. B., et al. (2013), Antarctica, Greenland and Gulf of Alaska land-ice evolution from an iterated GRACE global mascon solution, *J. Glac.*, *59*(216), 809–819, doi:10.3189/2013JoG12J147.

National Snow and Ice Data Center (2013), *Correction to ICESat data product surface elevations*. http://nsidc.org/data/icesat/correction-to-product-surface-elevations.html.

Rignot, E., J. Mouginot, and B. Scheuchl (2011), Ice flow of the Antarctic ice sheet, *Science*, *333*(6048), 1427–1430, doi:10.1126/science.1208336.

Shepherd, A., et al. (2012), A reconciled estimate of ice-sheet mass balance, *Science*, *338*(6111), 1183–1189, doi:10.1126/science.1128102.

Siegfried, M. R., et al. (2011), High-resolution ground-based GPS measurements show inter-campaign bias in ICESat elevation data, *IEEE Trans. Geosci. Rem. Sens.*, *49*(9), 3393–3400.

Zwally, H. J., et al. (2002), ICESat's laser measurements of polar ice, atmosphere, ocean and land, *J. Geod.*, *34*, 405–445, doi:10.1016/S0264-3707(02)00042-X.

Zwally, H. J., et al. (2011), Greenland ice sheet mass balance: Distribution of increased mass loss with climate warming; 2003–07 versus 1992–2002, *J. Glaciol.*, *57*(201), 88–102, doi:10.3189/002214311795306682.